# RECTANGULAR ROAD MARKING DETECTION WITH MARKED POINT PROCESSES

**Olivier Tournaire[1,2], Nicolas Paparoditis[2], Florent Lafarge[2]**

[1]UMLV / OTIG, 5, Bd Descartes, Champs-sur-Marne 77454 Marne-la-Valle CEDEX 2 - France
[2]IGN / MATIS, 2-4, Ave Pasteur, 94165 S$^t$-Mandé - France

{olivier.tournaire;nicolas.paparoditis;florent.lafarge}@ign.fr

**Commission III/5**

**KEY WORDS:** Road-marks, aerial images, RJMCMC, Simulated annealing, Stochastic geometry

**ABSTRACT:**

We propose in this article an energy minimization based approach to detect dashed lines of road markings from very high resolution aerial images ($<$ 20 cm). The strategy we presented in a previous work was based on the grouping of image features (i.e. segments) extracted from the images (reference, n.d.), but suffers from a few problems such as occlusions mainly due to cars or changing in illumination conditions like shadows areas produced by trees or buildings or low contrast due to worn out markings.
In order to obtain a more robust and reliable extraction of those objects, we have to find another approach which can take into account those observations. In this context, we use marked point process which are random variables whose realization are configuration of geometrical shapes (rectangle in our case). We use an energy formulation based on both an external and internal terms. A RJMCMC sampler coupled with a simulated annealing is used to find the optimal object configuration according to the proposed energy. Some results are shown on various aerial images in urban areas.

## 1 INTRODUCTION

Automatic road extraction has been a challenging topic since many years in the geographic and photogrammetric communities (Mayer et al., 2006). Road markings can be an interesting object for their update or completion in rural as in dense urban areas. In fact, they are useful to extract topological information such as intersections or semantic ones (i.e. road functionality, number of circulations lanes ...).
With a different goal, some authors use road markings informations in their system. Those objects have been considered particularly interesting for autonomous navigation of land vehicles (Charbonnier et al., 1997). Indeed, road marks are invariant elements and can easily be recognized by terrestrial based camera sensors in order to provide visual landmarks. They can then be used in a matching process in order to find or match a vehicle trajectory.

In an aerial context, only few papers addressed this topic. This is most probably due to the fact that this kind of objects are quite small related to the ground sampling distance of the images used for road extraction systems. They are however very structuring notably in urban areas where accurate road detection stays a vast challenge.
Many approaches have been developed for the extraction of complex road networks. Some of them lie on clues detection such as road marks which is a very good indicator of the attendance of road. For example, (Zhang, 2003) tries to find zebra-crossings with a colorimetric analysis in order to obtain the main road direction. (Hinz and Baumgartner, 2002), with a radiometric model of dashed lines extract those objects for the same purpose, also introducing geometric regularity analysis of the detected elements. A graph approach is presented in (Steger et al., 1997) to group road marks patterns. A best-first-search is performed and leads to find an optimal path in the graph to group those features. Closer to what we present in this paper, (Lacoste et al., 2005) detects road networks with a stochastic approach using marked point processes (segments objects). One should note that the method is extensible to various network forms. RJMCMC is also of interest in terrestrial photogrammetry for facades features extraction and interpretation (Mayer and Reznik, 2006, Brenner and Ripperda, 2006).
The strategy we will address in this article is based on the same approach. Our aim is to provide an energetic modeling of the dashed road marks lines. We will use marked point processes modeled by rectangular patterns. Each point of the process will stand for a strip of the lines we propose to extract. The method is fully automatic and is based on an homogeneous mathematical framework which provides robustness to the process. Such a technique is particularly interesting for the following reasons:

- it allows a modeling using simple geometric objects (rectangle),
- it allows the introduction of prior knowledge related to the object layout, which is particularly interesting for the management of occlusions and low contrast,
- the process converges towards the optimal solution for any initial configuration.

To present our algorithm we first have an overlook on marked point process. Then, we propose an energy formulation based on both a data term which measures the coherence between the objects configuration and the image, and a regularizing term which takes into account some interactions existing between neighboring objects. A RJMCMC sampler coupled with a simulated annealing is used to find the optimal object configuration according to the proposed energy. Finally, results on Amiens downtown are presented.

## 2 MODEL DEFINITION

We now present how we build the energy of the model. Before going into details, we come back on essentials aspects of marked points processes.

### 2.1 Marked Point Processes

Point processes have been introduced in image processing by (Baddeley and Van-Lieshout, 1993) so as to detect an unknown number of objects in an image. In this theoretical frame, the problem is to locate the objects in the image and to measure them. Such modeling has been applied to numerous problematics in many research areas, as for example buildings reconstruction (Lafarge et al., 2006) or road extraction (Lacoste et al., 2005) from satellite or aerial imagery.
As show on figure 1, dashed lines are composed of several rectangular objects separated from each others with a fixed distance depending on the road type or functionality. The rectangles also have the same width for a given line. To describe the base object of our process, we need three parameters : its position $(x_i, y_i)$ and its orientation $\theta_i$ (see figure 2). The width $w$ and the length $h$ of the rectangle are fixed according to the image GSD. In practice, $h$ corresponds to 15 cm and $\omega$ is 1.5 m or 3 m according to the scene.

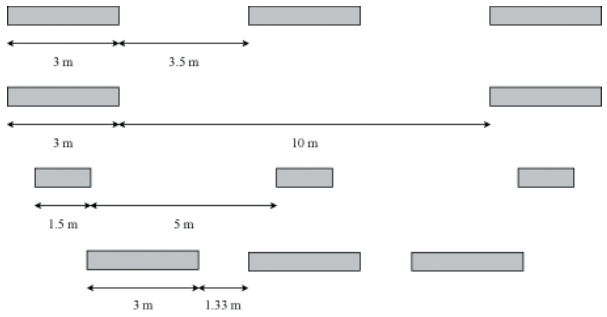


Figure 1: Geometric characteristics of the discontinuous lines objects'.

To summarize, an object of our marked process is distributed in the space $\mathcal{M} = [0; X_{max}] \times [0; Y_{max}] \times [0; \pi]$. $(x_i, y_i) \in [0; X_{max}] \times [0; Y_{max}]$ ... and $\theta_i$ stands in the interval $[0; \pi]$. A realization of our marked point process is an element of $\mathcal{M}^n$, $n \in \mathbb{N}$.

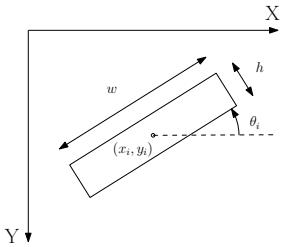


Figure 2: The object $i$: the point $(x_i, y_i)$ and its associated mark $\theta_i$.

### 2.2 Energy formulation

We aim at proposing a model for dashed lines detection of the road marking. We will thus have to build an energetic formulation of the modeling. The global energy $\mathcal{U}$ of the model is composed of two terms - a data attachment term and a regularizing term - following equation 1:

$$\mathcal{U} = \beta \mathcal{U}_{ext} + (1 - \beta)\, \mathcal{U}_{int} \tag{1}$$

Each term is described in the next paragraphs. First of all, we need to describe the base objects of the process and their associated marks.

#### 2.2.1 Internal energy $\mathcal{U}_{int}$

The internal term allows to introduce prior knowledge concerning the object layout. This regularizing term is developed through interactions existing between neighboring objects. We first need to setup a neighborhood relationship.

**Neighborhood**
Two objects $i$ and $j$ are said neighbors if they verify the following equation (equation 2).

$$i \sim j \Leftrightarrow d\left(\overline{i}, \overline{j}\right) \leq r_{\mathcal{D}} \tag{2}$$

where $\overline{i}$ is the center of the object $i$ and $r_{\mathcal{D}} = w + d_{inter-stripes} + \epsilon_{\mathcal{D}}$. $d_{inter-stripes}$ directly comes from the specifications and $\epsilon_{\mathcal{D}}$ is used to allow a tolerance on the distance between two consecutive stripes.

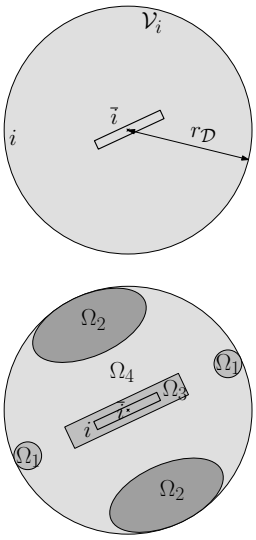


Figure 3: The neighborhood $\sim$ of an object $i$ (top) and its different interest areas (bottom).

**Interaction principle**
The internal term is computed for pairs of objects in interaction. In other words, if $x$ is a configuration of objects, the internal term is expressed as:

$$\mathcal{U}_{int}(x) = \sum_{i \sim j} \mathcal{U}_P(i, j) \tag{3}$$

We detail $\mathcal{U}_P$ in the following. Interactions have to be differentiate in accordance with the relative orientation and position of the objects inside the neighborhood (see figure 3 and equations 4 and 5). The neighborhood is thus divided into several areas: an attractive one ($\Omega_1$) which is the union of two discs, a neutral one ($\Omega_2$) composed of two ellipses and a repulsive one ($\Omega_3 \cup \Omega_4$).

$$\mathcal{U}_P(i, j) = \begin{cases} \mathcal{U}_P^*(i, j) & \text{if } |\theta_i - \theta_j| \leq \epsilon_\theta \\ \mathcal{A} & \text{otherwise} \end{cases} \tag{4}$$

$$\mathcal{U}_P^*(i, j) = \begin{cases} \mathcal{B} & \text{if } \overline{j} \in \Omega_1 \\ 0 & \text{if } \overline{j} \in \Omega_2 \\ \mathcal{C} & \text{if } \overline{j} \in \Omega_3 \\ \mathcal{D} & \text{if } \overline{j} \in \Omega_4 \end{cases} \tag{5}$$

If two neighbors objects have a high angular difference, they are penalized and are affected with a regularizing value of $\mathcal{A}$. Otherwise, four cases are distinguished. In order to highly penalize

objects overlapping, $\Omega_3$ is defined as a rectangle surrounding the base object $i$. If an object $j$ lies in this area, the relation between $i$ and $j$ is set to the maximum value. In the remainder of the repulsive area, the value ($\mathcal{D}$) is a little low in order to avoid disadvantage too much objects between circulation lanes (like directional arrows). In $\Omega_2$, the neutral area, the value of the energy is set to 0. This is useful when the road is composed of parallel circulation lines as shown on figure 4.

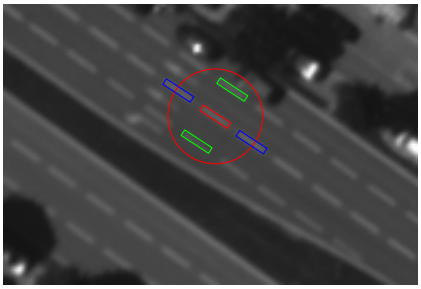

Figure 4: Illustration of the problem of parallel circulation lanes when the neighborhood is not parted with $\Omega_2$. The base object $i$ is the red one. Blue ones are located in the attractive area. If $\Omega_2$ is not defined, the green objects would have been affected a high energy value.

Finally, if $j$ stands in $\Omega_1$, the objects $i$ and $j$ are considered to be attracted each other and they are affected with the lowest regularizing energy value. The closest $\overline{j}$ is from the center of $\Omega_1$, the lowest the energy is. The energy is defined thanks to the function $f$ (equation 6) inspired by a Laplace distribution:

$$f(x) = \frac{1}{2b} e^{-\frac{|x-t|}{b}} \tag{6}$$

### 2.2.2 External energy $\mathcal{U}_{ext}$

The data term indicates the likelihood of the objects of the model in relation with the image. With the same notations as in equation 3, we have:

$$\mathcal{U}_D(x) = \sum_{i \in x} \mathcal{U}^i_{int} \tag{7}$$

were $\mathcal{U}^i_{int}$ is the external energy of each object of the $x$ configuration.
For dashed lines modeling, we simply have noticed that the strips forming a line are clear objects on a darker background. We also make the hypothesis that pixels within the objects and in their adjacent neighborhood are homogeneous. From this, the external energy is defined in terms of region analysis.
In order to avoid thresholds, we use a statistical criterion to decide if two regions are radiometrically distinct. This way, we define for an object two kinds of points: internal and external ones (see figure 5).

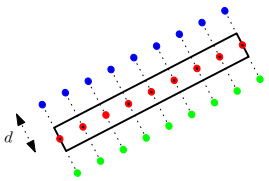


Figure 5: Inner and outer points of an object.

We thus have three sets of pixels obtained by slicing the rectangle. In order to test if the object is well positioned, we compute the Mahalanobis distance (Mahalanobis, 1936) between each set of outer points and the inner points. For two regions $\mathcal{R}_1$ and $\mathcal{R}_2$, it is given by equation 8.

$$d_{Maha.}(\mathcal{R}_1, \mathcal{R}_2) = n \left(\overline{p^{\mathcal{R}_1}} - \overline{p^{\mathcal{R}_2}}\right)^2 \left[\sum_{j \in \{\mathcal{R}_1, \mathcal{R}_2\}} \sum_{k=1}^{n} \left(p^j_k - \overline{p^j}\right)^2\right]^{-1} \tag{8}$$

where $n$ is the number of pixels in a region, $\overline{p^{\mathcal{R}_1}}$ (*resp.* $\overline{p^{\mathcal{R}_2}}$) is the radiometric mean of the internal pixels (*resp.* external) and $p^j_k$ is the radiometry of the pixel $k \in \{1, \ldots, n\}$ from the region $j = \{\mathcal{R}_1, \mathcal{R}_2\}$. The Mahalanobis distance follows a $\chi^2$ law. In our case, it has two degrees of freedom. Thus, with a risk $\alpha$, it is possible to obtain from the $\chi^2$ distribution function a threshold which allows to decide if the regions we are currently testing are radiometrically dissimilar. From this, the external energy is given by equation 9.

$$\mathcal{U}^i_{ext}\left(d_{Maha.}(in, out), t_{\chi^2}\right) = -\frac{d_{Maha.} - t_{\chi^2}}{\sqrt{1 + \frac{\left(d_{Maha.} - t_{\chi^2}\right)}{2}}} \tag{9}$$

This function has a high derivative around $t_{\chi^2}$ and is null when the Mahalanobis distance is equal to $t_{\chi^2}$. When inner and outer regions are dissimilar, the numerator takes a high positive value and the energy is then highly negative. The shape of the function is given on figure 6 where the $x$-coordinate is the Mahalanobis distance and the $y$ one is the data energy value.

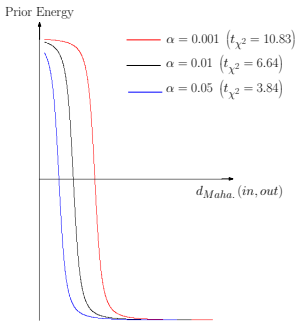


Figure 6: Data energy value for different error risks $\alpha$.

### 2.2.3 Parameters settings

**Physical parameters**
This kind of parameters have a physical interpretation in the application. They are fixed according to the scene.
For example, $w$ and $d_{inter-stripes}$ are used is the computation of the radius of the $\sim$ relation. They directly depend on the kind of dashed line we want to extract. The different possible values are defined from the specifications as show on figure 1.

**Weights and thresholds**
Data and regularizing terms are weighted one compared to the other, respectively with a factor $\beta$ and $1 - \beta$. $\beta$ is tuned by *"trial and errors"*. Let us say that the data term is around 60% to 75% of the total. A better way to obtain this value is discussed in the conclusion.
Some thresholds are also necessary in our model. The first one, $\epsilon_d$, is set in order to have a tolerance on the radius of the $\sim$ relation. We need it because specifications are strong, but sometimes, they are not respected and the distance between two consecutive stripes can be a little bit more than what it should be. The other threshold, $\epsilon_\theta$, is used when computing internal energy. It leads to consider a particular relation between two stripes having a weak angular difference. In our application, we use $\epsilon_d = 0.5$ m pixels

and $\epsilon_\theta = \frac{\pi}{8}$.

## 3 OPTIMIZATION

We aim at finding the configuration of objects which minimizes the energy $\mathcal{U}$. This is a non convex optimization problem in a high and variable dimension space since the number of objects is unknown.

### 3.1 RJMCMC sampler

The Reversible Jump Markov Chain Monte Carlo (RJMCMC) algorithm (Geyer and Møller, 1994, Green, 1995) is well adapted to our problem. Several papers have shown the efficiency of the RJMCMC sampler for the marked point processes problems (Geyer and Møller, 1994, Lacoste et al., 2005). To do so, an non normalized density $h(.)$ is defined through the energy $\mathcal{U}$ thanks to the Gibbs relation:

$$h(.) = \exp -\mathcal{U}(.) \tag{10}$$

The RJMCMC sampler consists in simulating a discrete Markov Chain $(X_t)_{t\in\mathbb{N}}$ on $\mathcal{R}$ the space of the configurations having $\pi$ as invariant measure (specified by the density $h(.)$) which performs "small jumps" between spaces of variable dimensions respecting the reversibility assumption of the chain. Propositions are based on "small jumps" which means only one object of the global configuration will be concerned by a new proposition. One of the main advantages of such a sampler is that the chain asymptotically converges towards $\pi$ for any initial configuration $X_0$. It means that we do not need specific initial object configuration. The jumps are proposed according to various kinds of kernels $Q_m$ specified in the following:

- **Birth and death** kernels allow to informally add / remove an object in / from the current configuration. These two transformations, which correspond to jumps in spaces of higher (birth) / lower (death) dimension, guaranty that the Markov Chain visits the whole configuration space. However, it is important to define relevant moves in order to speed up the convergence of the Markov chain.

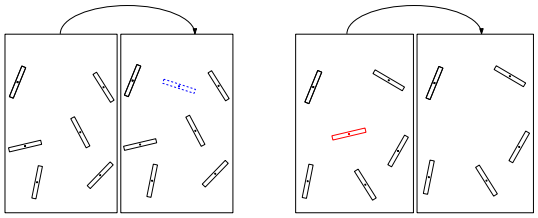

Figure 7: Birth uniform (left) and death uniform (right).

- **Birth and death in a neighborhood** kernels, introduced by (Green, 1995), consists in adding / removing an object in the neighborhood of a current object. In other words, it allows to propose objects in the areas of interest.

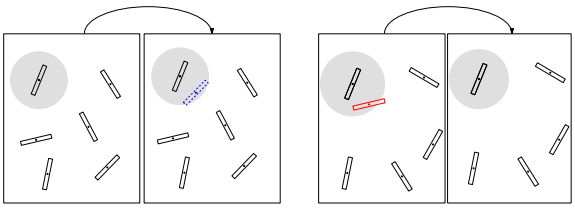

Figure 8: Birth (left) and death (right) in a neighborhood.

- **Perturbation** kernels are composed of rotation and translation moves. This kind of kernels is very useful for adjusting the positioning of the objects.

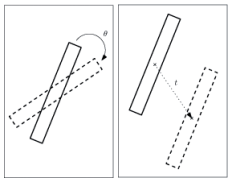

Figure 9: Rotation and translation propositions.

Let us summarized the RJMCMC sampler. At iteration $t$, if $X_t = x$:

- Choose the kernel $Q_i(x, .)$ with probability $q_i$
- According to $Q_i$, propose a new state $y$
- Take $x^{(t+1)} = y$ with probability:

$$\min\left(\frac{\pi(dy)}{\pi(dx)}\frac{Q_i(y,dx)}{Q_i(x,dy)}, 1\right)$$

- And take $x^{(t+1)} = x$ otherwise

**Algorithm 1**: RJMCMC sampler algorithm

### 3.2 Simulated annealing

A simulated annealing is used to ensure the convergence process: the density $h(.)$ is substituted by $h(.)^{\frac{1}{T_t}}$ where $T_t$ is a sequence of temperatures which tends to zero as $t$ tends to infinity. The simulated annealing allows to theoretically ensure the converge to the global optimum for all initial configuration $x_0$ using a logarithmic temperature decrease. In practice, we prefer using a geometrical decrease which is faster and gives an approximate solution close to the optimal one. The initial and final temperatures are estimated through the variation of the energy, using the work of (White, 1984).

## 4 RESULTS

We now present some results of our algorithm with aerial images acquired on the downtown of Amiens with a GSD of 25 cm.
Figure 10 shows the evolution of the process on a simple example and its ability to deal with curved structures. At the beginning of the algorithm (i.e. when the temperature is high - see 10 a)) the process explores the density modes. When the temperature decreases, the process begins to be selective (see 10 d) and e)) and the rectangles begins to be well located. At low temperature (see 10 g) and h)) the configuration is close to the optimal one: it consists in adjusting the parameters of the objects of the configuration.
Some statistics associated with the results of figure 10 are presented on figure 11. They show how does the configuration evolves and tends to converge.

Figure 12 shows an other example of the results obtained with our algorithm. Some details illustrate how the algorithm overcome difficulties of vehicles occlusions or shadows area due to trees. However, on this example, some rectangles are missing, and some others are detected where no pattern exist. We can certainly cope with those miss detection and false detection with tuning more precisely the weights of the both energy terms.

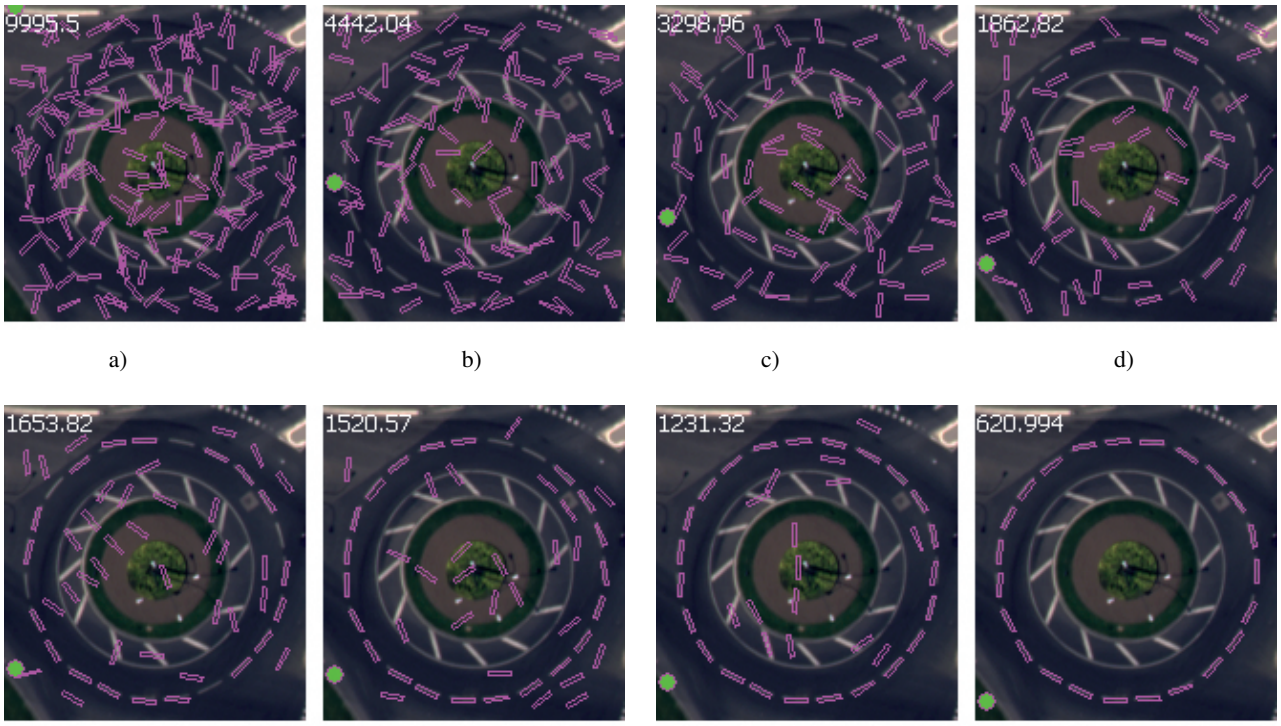


Figure 10: The algorithm in evolution (the figures correspond to the unormalized temperature used in the simulated annealing). Amiens - GSD 25 cm. From left to right and top to bottom : initial configuration - the firsts steps - a few objects find their position - more and more objects are well positioned - all objects are on road marks but a few are still present with a bad position - finally, all objects are well positioned and no more objects are misplaced.

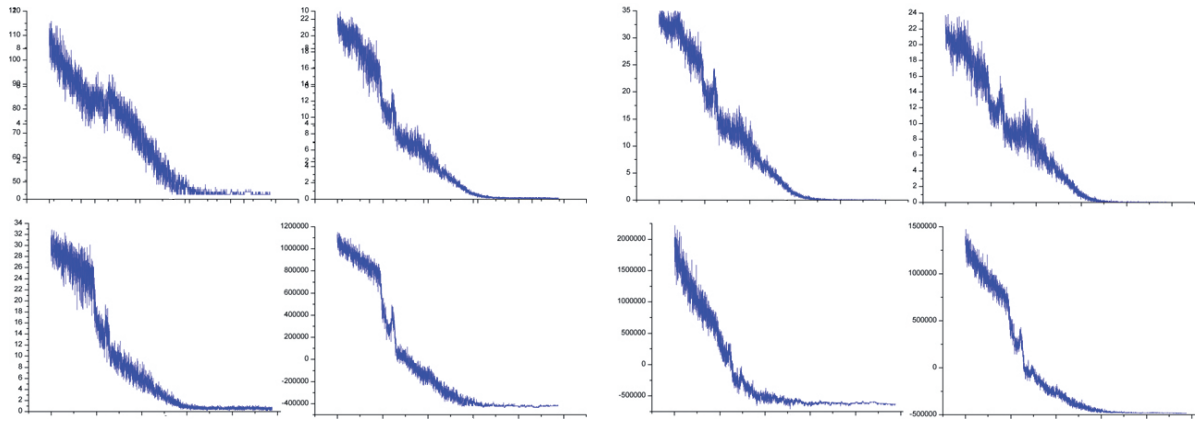

Figure 11: Statistics associated with the result show on figure 10. From left to right and top to bottom : number of objects - global acceptance rate - birth acceptance rate - death acceptance rate - perturbation acceptance rate - external energy - internal energy - total energy.

Figure 12: The algorithm in evolution. Amiens - GSD 25 cm

## 5 CONCLUSION AND FUTURE WORKS

We have presented in this paper an algorithm based on stochastic geometry to detect rectangular road marking. Marked point processes are well adapted to detect this kind of objects fully automatically and without an initialization. Using simulated annealing with a RJMCMC sampler for the model optimization allows us to choose randomly the initialization without any impact on the result. Prior knowledge lead to the detection of strictly linear or curved structures in aerial images. It also allows us to deal with total occlusions due to vehicles or partial ones due to shadows, thus bringing a high level of robustness to the model.
However, some issues have to be studied in the future. The first one will be to introduce in the regularizing term knowledge in order to take into account changes in the lines structure. Next, it will be interesting to try to find the weighting coefficients with an automatic algorithm approach such as *Expectation Maximization* (Dempster et al., 1977) instead of tuning it by *trial and error*. Finally, in order to reduce computation time, it could be interesting to develop data driven kernels allowing to reduce the search space. Investigations on this point are currently being studied.

## REFERENCES


Baddeley and Van-Lieshout, M., 1993. Stochastic geometry models in high-level vision. Statistics and Images 1, pp. 233–258.

Brenner, C. and Ripperda, N., 2006. Extraction of facades using RJMCMC and constraint equations. In: International Archives of Photogrammetry and Remote Sensing, Vol. XXXVI - 3, pp. 155–160.

Charbonnier, P., Diebolt, F., Guillard, Y. and Peyret, F., 1997. Road markings recognition using image processing. In: IEEE Conference on Intelligent Transportation System, Vol. 1, pp. 912–917.

Dempster, A., Laird, N. and Rubin, D., 1977. Maximum likelihood from incomplete data via the EM algorithm. Journal of the Royal Statistical Society B39, pp. 1–38.

Geyer, C. and Møller, J., 1994. Simulation and likelihood inference for spatial point processes. Scandinavian Journal of Statistics 21, pp. 359–373.

Green, P., 1995. Reversible jump markov chain monte carlo computation and bayesian model determination. Biometrika 82, pp. 711–732.

Hinz, S. and Baumgartner, A., 2002. Urban road net extraction integrating internal evaluation model. In: ISPRS Commission III Symposium on Photogrammetric Computer Vision, Vol. XXXIV - Part 3A, Graz, Austria, pp. 163–168.

Lacoste, C., Descombes, X. and Zerubia, J., 2005. Point processes for unsupervised line network extraction in remote sensing. IEEE Trans. Pattern Analysis and Machine Intelligence 27(10), pp. 1568–1579.

Lafarge, F., Descombes, X., Zerubia, J. and Pierrot-Deseilligny, M., 2006. An automatic building reconstruction method : A structural approach using high resolution images. In: Proc. of IEEE International Conference on Image Processing, Atlanta - USA.

Mahalanobis, P., 1936. On the generalized distance in statistics. In: Proc. Nat. Inst. Sci. India, Calcutta - India.

Mayer, H. and Reznik, S., 2006. MCMC linked with implicit shape models and plane sweeping for 3D building facade interpretation in image sequences. In: International Archives of Photogrammetry and Remote Sensing, Vol. XXXVI - 3, pp. 130–135.

Mayer, H., Hinz, S., Bacher, U. and Baltsavias, E., 2006. A test of automatic road extraction approaches. In: International Archives of Photogrammetry and Remote Sensing, Vol. XXXVI - 3, pp. 209–214.

reference, A. A., n.d.

Steger, C., Mayer, H. and Radig, B., 1997. The role of grouping for road extraction. In: A. Gruen, E. Baltsavias and O. Henricsson (eds), Automatic Extraction of Man-Made Objects from Aerial and Space Images (II), Birkhäuser Verlag, Basel, Switzerland, pp. 245–256.

White, S., 1984. Concepts of scale in simulated annealing. In: Proceedings IEEE, International Conference on Computer Design, Port Chester, pp. 646–651.

Zhang, C., 2003. Updating of cartographic road databases by image analysis. PhD thesis, Institute of Geodesy and Photogrammetry, Zurich.